

EVOLUTION OF PLASTIC STRAINS IN DISSIMILAR WELD OF STAINLESS STEEL TO CARBON STEEL

Eslam Ranjbarnodeh*, Mehdi Farajpour

Ghiamdasht Branch, Islamic Azad University, Tehran, Iran

Received 16.08.2011

Accepted 15.09.2011

Abstract

In the current study, a verified thermo-mechanical model is utilized to investigate the evolution of stresses and strains in dissimilar TIG welds of low carbon and ferritic stainless steels. The histories of stresses, elastic and plastic strains of the both base metals are analyzed. The results show that the magnitude of plastic strains increases, as the yield strength of the base metal decreases while the higher amount of plastic strains are produced in the similar joint of the stainless steel.

Key words: Dissimilar joint; Plastic strain; Strain evolution; Carbon steel; Stainless steel

Introduction

In arc welding processes residual stresses are produced within the welded metal due to the high local temperature field and severe temperature gradients [1]. Dissimilar joints are made between two materials that are significantly different in chemical and/or mechanical senses. When dissimilar metals are joined by a fusion welding process such as TIG welding operations, alloying between the base metals and filler metal becomes a major point and as a result the weld metal may show totally different mechanical properties as well as distribution of residual stress within the weldment is achieved [2]. Till now, there have been a few published studies about residual stresses in similar as well as dissimilar arc welding operations. For instance; Paradowska *et al.* [3] investigated the effect of heat input on residual stresses distribution. They found that the heat input affects the value and distribution of residual stresses in the specimen while the transverse residual stresses were about half of the maximum value of longitudinal stresses. Teng *et al.* [4] developed a model to simulate the effects of welding speed, specimen size, mechanical constraint and preheating on residual stresses. Ranjbarnodeh *et al.* [5] studied the effect of heat input on residual stresses in dissimilar joints. Their

* Corresponding author: Eslam Ranjbarnodeh, islam_ranjbar@yahoo.com

results showed that the magnitude of stresses at the weld center line increases with increasing the welding speed.

The final state of plastic strains and other variables have been studied in the above mentioned papers, but analysis of plastic strain history is also important to garner insight into the formation mechanism of plastic strains. The analysis also enables better understanding of welding residual stresses. There are few researches investigating the history of plastic strains in the welded structures. Fang *et al.* [6] studied the formation mechanism of longitudinal residual stress and plastic strain in the welding of low carbon steel. Their results revealed that the tensile plastic strain generated in the cooling process cannot counteract the compressive plastic strain generated in the heating process, resulting in the remaining of the compressive plastic strain in the weld after welding. Cheng *et al.* [7] used FEM to simulate the in plane shrinkage strains and welding distortion in thin wall structures.

Regarding the published works on the evolution of plastic deformation in welding processes, further studies are required to acquire a more complete understanding about the welding plastic strains in dissimilar joints. In order to achieve a comprehension of this problem based on a verified model [8] evolution of plastic strain in dissimilar joint of stainless steel to carbon steel was studied in the present work and the results were compared with the similar joints of stainless steel.

Mathematical Model

Prediction of temperature field in welding process is one of the main factors in determining welding residual stresses and plastic strains. Accordingly, the problem of heat conduction in the welded structure must be solved. Thus, the following equation can be used to describe temperature variations inside the parts are being welded:

$$\frac{\partial}{\partial x} \left(k \frac{\partial T}{\partial x} \right) + \frac{\partial}{\partial y} \left(k \frac{\partial T}{\partial y} \right) + \frac{\partial}{\partial z} \left(k \frac{\partial T}{\partial z} \right) = \rho C \frac{\partial T}{\partial t} \quad (1)$$

where T is the temperature, k is the thermal conductivity, C is the specific heat, ρ is the density, t represents welding time, and z , x and y show welding direction, transverse direction and thickness direction, respectively. At the beginning of the process ($t=0$ sec), the entire model was at the ambient temperature. During the welding process, the following boundary conditions were used. Convection-conduction boundary conditions were assumed on surface boundaries except for the region affected by the moving arc, as presented in Eq. 2:

$$-k \frac{\partial T}{\partial n} = h(T - T_a) \quad (2)$$

where “ n ” denotes the normal direction to the surface boundary, T_a is the ambient temperature and h is convection heat transfer coefficient. Convective coefficient was taken as 15 W/m²K for the surfaces in contact with ambient air. The bottom surface of is in contact with the top surface of the welding fixture. This backing plate, being thick (12mm), acts as a heat sink for the bottom surface. Therefore, the convection coefficient was estimated as 800 W/m²K for this region [9].

At the top surface of the model in the region influenced by the moving welding arc the boundary condition is given as Eq. 3:

$$k \frac{\partial T}{\partial y} = q(r) = \frac{\eta VI}{2\pi r'^2} \exp\left[-\frac{1}{2}\left(\frac{r}{r'}\right)^2\right] \quad (3)$$

where “n” stands for the normal direction to the surface boundary, $q(r)$ is surface heat flux that was used to simulate the energy transfer from the arc into the surface of the workpiece, η is welding process efficiency, V is welding voltage (13V), I is welding current, T_a is the ambient temperature, “r” is the distance from the center of heat source and “ r' ” is the Gaussian distribution parameter which is the radius of area to which 95% of energy is entered [1]. In this work, “ r' ” was assumed to be 1.5 mm and η was taken as 0.6 [10]. The used mesh system is displayed in Fig. 1.

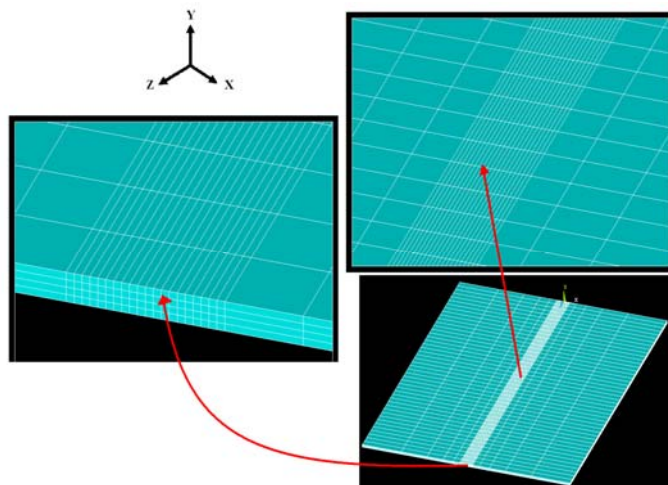


Fig. 1. The employed mesh system.

At the same time, the mechanical behavior of the weldment should be determined by equilibrium equation as mentioned in Eq. 4.

$$\sigma_{ij,j} + b_i = 0 \quad (4)$$

where σ_{ij} is the Cauchy stress tensor and b_i is the body force (temperature) vector which are calculated from the thermal analysis. Note that the thermo-elastic-plastic behavior, based on the Von Mises yield criterion and the isotropic strain hardening rule, is considered in the model. In the mechanical part of the simulation, the substantial boundary conditions were $u(0,0,0)=0$ for the origin of the coordination system and the normal displacement, u_y , equals zero for the bottom surface of the welded plates because the top surface of the backing plate acts as a rigid fixture for this surface. Accordingly, the constitutive equation can be written as following [4]:

$$d\sigma = D^{ep} d\varepsilon - C^{th} dT \quad (5)$$

$$\mathbf{D}^{ep} = \mathbf{D}^e + \mathbf{D}^p \quad (6)$$

where \mathbf{D}^{ep} is the elastic-plastic stiffness matrix, \mathbf{D}^e is the elastic stiffness matrix, \mathbf{D}^p is the plastic stiffness matrix, \mathbf{C}^h denotes the thermal strain vector, $d\sigma$ is the vector of stress increment, $d\varepsilon$ is the vector of strain increment and dT is the temperature increment.

Experimental data

It is worth noting that in short samples, 5670 elements and 7130 nodes are used while for the longer samples, 11340 elements and 14105 nodes have been used in the analysis. In addition, temperature-dependent material properties were employed for both stainless steel and low carbon steel parts (Tables 1 and 2 and Fig. 2). The specific heat of AISI409 was assumed to be 460 J/kg.K [11]. Furthermore, to take the effect of fluid flow in the weld pool into account, the thermal conductivity was assumed to increase linearly above the melting point by a factor of about three [12, 13]. The thermal expansion coefficient of low carbon steel and stainless steel were given to be 11.7×10^{-6} and 12×10^{-6} , respectively. The results of model were validated using X-ray diffraction method [8]. TIG welding was applied and the used welding parameters in this study are presented in Table 3.

Table 1. Thermo-physical properties of carbon steel [8].

Temperature($^{\circ}\text{C}$)	Thermal Conductivity (W/m.K)	Temperature ($^{\circ}\text{C}$)	C(J/kg.K)
20	51.5	20	425
800	29.7	675	846
1500	29.7	700	1139
2000	90	730	1384
		750	1191
		1000	779
		1500	400
		2860	400

Table 2. Thermo-physical properties of stainless steel [8].

Temperature($^{\circ}\text{C}$)	Thermal Conductivity (W/m.K)	Temperature($^{\circ}\text{C}$)	C(J/kg.K)
20	25	20	460
500	30		
1400	30		
2000	90		

Table 3. The used TIG welding parameters.

Sample	Current (A)	Length (mm)	Speed (mm/s)	Voltage (V)	The base metals
Dissimilar joint	120	450	3.56	13	Stainless steel/Carbon steel
Similar joint	120	450	3.56	13	Stainless steel/ Stainless steel

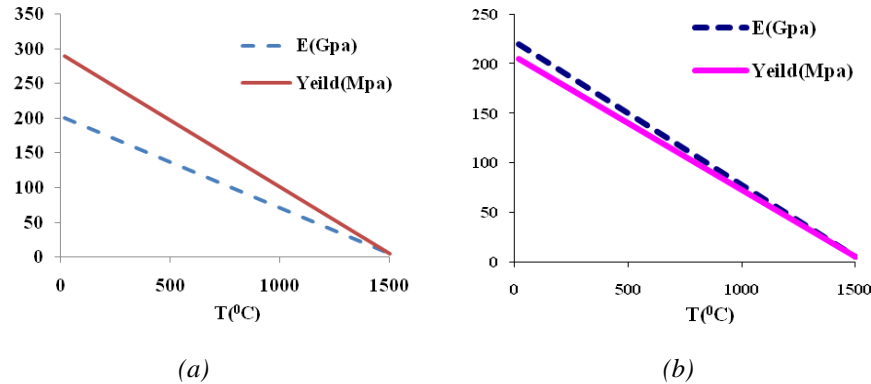


Fig. 2. The mechanical properties of, a) carbon steel, b) stainless steel.

Results and discussion

Fig. 3 shows the temperature cycles at different points of the welded sample. It is shown that the different thermo-physical properties of the base metals resulted in different temperature variations. Thermal conductivity of carbon steel is higher than the stainless steel, which in turn, caused higher temperatures at the stainless steel side of the weld [8].

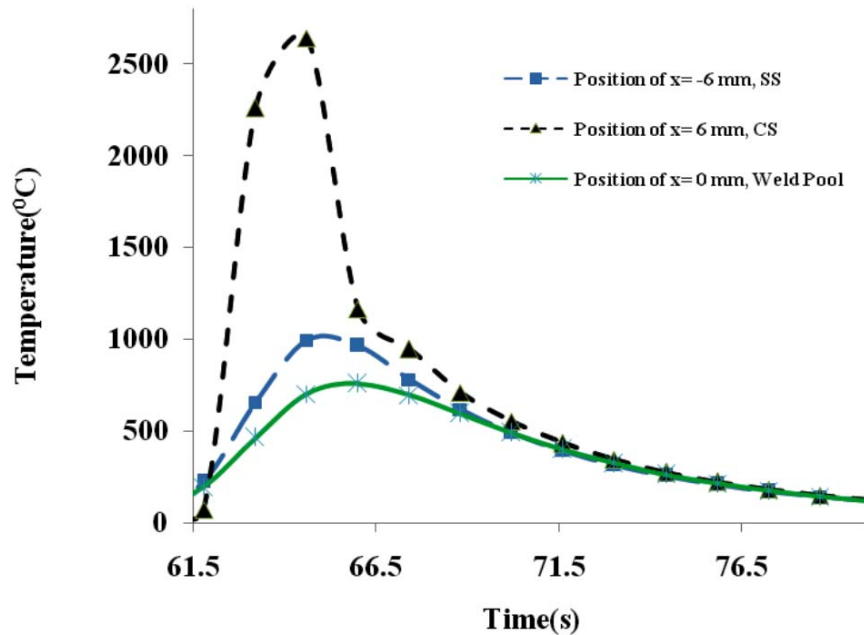


Fig. 3. The temperature cycles at different points of the welded sample [8].

Fig.4 shows the transient stresses at two points with the same distance of the weld center line. As it is seen during passing the welding heat source both of the base metals experience the compressive stresses.

However, tensile stresses occur on the cooling stage. The magnitudes of these stresses are somehow constant during holding in the fixture. After removing the fixture a part of stress will be released and accordingly the amount of stress is decreased. The state of stress at the final point shows the welding residual stresses. In general, welds undergo yielding in the process of cooling after welding; then tensile residual stresses, which are generated by the resistance of the material against contraction by cooling after welding, remain there [5].

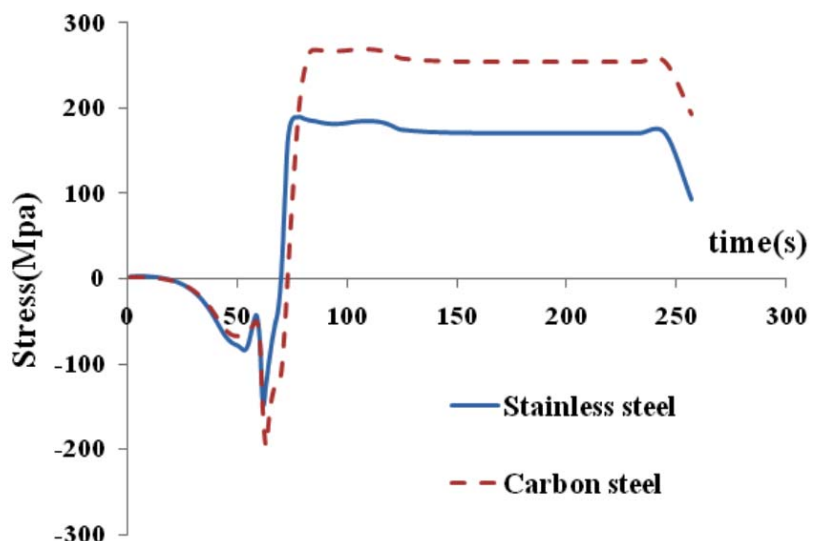


Fig. 4. The history of stress at two points of dissimilar weld.

The stainless steel with the lower yield strength cannot tolerate welding stresses and yields at the lower stresses. This phenomenon releases stresses and therefore the lower amount of residual stresses is remained in the stainless steel. The history of plastic strain for the base metals is presented in Fig. 5.

Against the plastic strain, the higher values of plastic strains are found for the stainless steel. As mentioned above, it can be due to the lower yield strength of the stainless steel. Another possible reason is the different peak temperatures for the used base metal. The lower thermal conductivity of the stainless steel results in the higher temperature that causes the higher amount of plastic strain. To study the effect of dissimilarity on magnitude of plastic strain, a similar joint of the stainless steel was simulated and its results were compared with correspondent dissimilar joint, depicted in Fig. 6. As it is seen, similar joint shows the higher amounts of plastic strains which may be attributed to the absence of carbon steel in this joint as a heat absorbent.

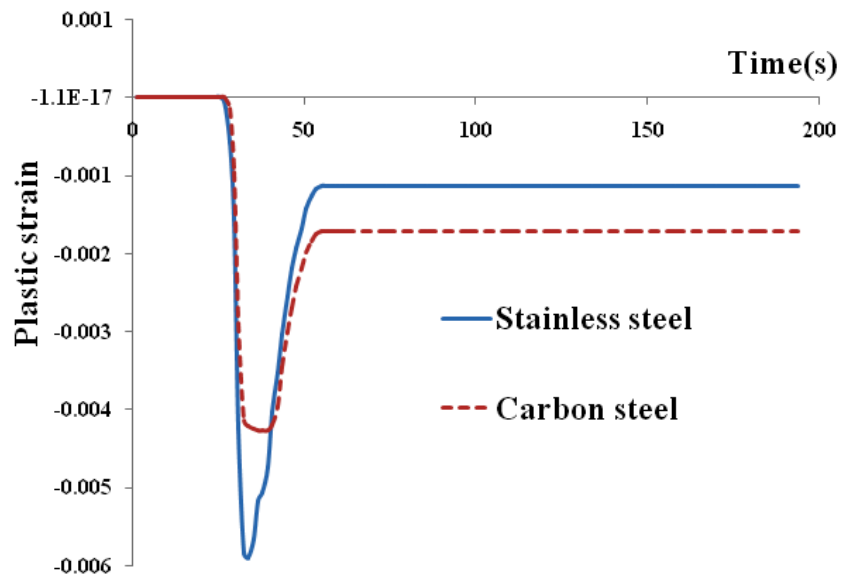


Fig. 5. The history of plastic strain at two points of dissimilar weld.

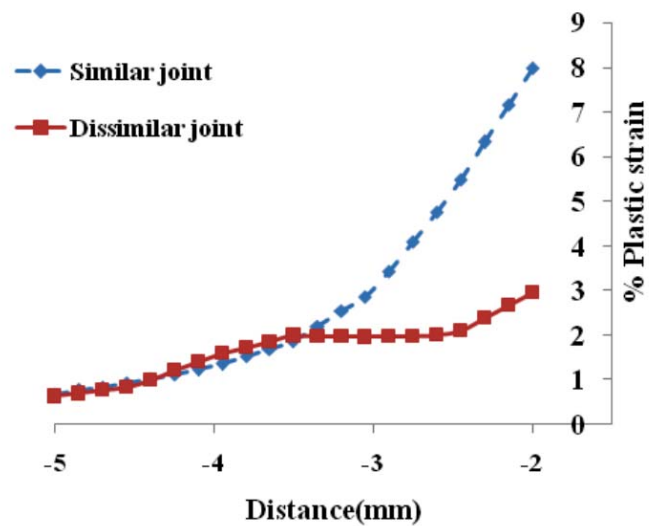


Fig. 6. The effect of dissimilarity on magnitude of plastic strain.

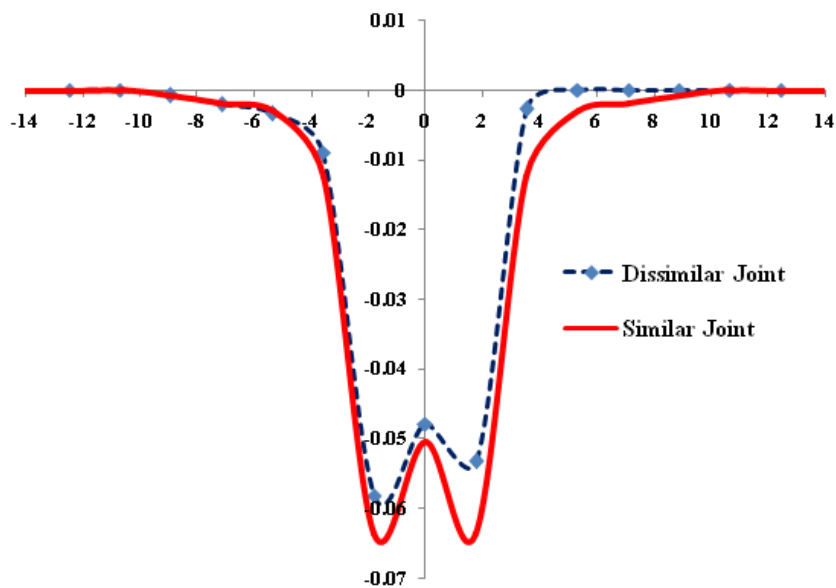


Fig. 7. The distribution of plastic strain along the x-axis.

Therefore, the similar joint will experience the higher temperature and this means the higher plastic strain. The distribution of plastic strain along the x-axis is shown in Fig. 7. This figure exhibits that the similar joint has the wider plastic strain compared to the dissimilar joint. It can be due to the lower conductivity of the stainless steel.

Conclusions

In this work, based on a verified model, the evolution of thermo mechanical behavior of dissimilar TIG welds of low carbon and ferritic stainless steels was studied. The stress, elastic and plastic strain cycles of different points of the joints of the both base metals were analyzed. Also, a similar joint was simulated to compare with the dissimilar joint. The results showed that:

1. The base metal with the lower yield strength shows the higher amount of plastic strain.
2. The lower thermal conductivity of the stainless steel causes the higher peak temperature and plastic strain.
3. In the similar joint, the absence of carbon steel, as a heat absorbent, causes the higher peak temperature and plastic strain.
4. The base metal with lower thermal conductivity shows the wider plastic zone.

References

- [1] S. Kou, *Welding Metallurgy*, John Wiley & Sons, New Jersey, 2003.
- [2] AWS Welding handbook, Vole 4, Ch 12, 1997.

- [3] A.M. Paradowska, J.W. H.Price, R. Ibrahim, T.R. Finlayson, Journal of Achievements in Materials and Manufacturing Engineering, 17(2006) 385-388.
- [4] T. Teng, C. Lin, Int. J. Press. Vessels Pip. 75(1998) 857–864.
- [5] E. Ranjbarnodeh , S. Serajzadeh , A.H. Kokabi, A. Fisher, S. Hanke, Int. J. Adv. Manuf. Technol. 55(2011) 649-656.
- [6] H.Y. Fang, X. Zhang, H. Yang, X. Liu, Q. Shen, Front. Mater. Sci. Chin. 3(2009) 75–77
- [7] W. Cheng, In-Plane shrinkage strains and their effects on welding distortion in thin wall structures. PhD Thesis. The Ohio State University, 2005.
- [8] E. Ranjbarnodeh, S. Serajzadeh, A.H. Kokabi, A. Fisher. J. Mater. Sci. 46(2010) 3225-3232.
- [9] R.A. Mufti, Mechanical and microstructural investigation of weld based rapid prototyping. PhD Thesis. Ghulam Ishaq Khan Institute of Engineering Sciences and Technology, Faculty of Mechanical Engineering, 2008.
- [10] H.R. Saedi, Transient response of plasma arc and weld pool geometry for GTAW process, PhD Thesis. Massachusetts Institute of Technology, 1983.
- [11] M. Abid, M. Siddique, Int. J. Press. Vessels Pip. 182(2005) 860–870.
- [12] B. Taljat B. Radhakrishnan B. Zacharia, Mater. Sci. Eng., A. 246(1998) 45–54.
- [13] A. De, T. DebRoy, J. Appl. Phys. 195(2004) 5230-5239.